

# A MORTON-TYPE SPACE-FILLING CURVE FOR PYRAMID SUBDIVISION AND HYBRID ADAPTIVE MESH REFINEMENT

DAVID KNAPP\*, JOHANNES ALBRECHT HOLKE†, THOMAS SPENKE‡, AND  
CARSTEN BURSTEDDE§

## Abstract.

The forest-of-refinement-trees approach allows for dynamic adaptive mesh refinement (AMR) at negligible cost. While originally developed for quadrilateral and hexahedral elements, previous work established the theory and algorithms for unstructured meshes of simplicial and prismatic elements. To harness the full potential of tree-based AMR for three-dimensional mixed-element meshes, this paper introduces the pyramid as a new functional element type; its primary purpose is to connect tetrahedral and hexahedral elements without hanging edges. We present a well-defined space-filling curve (SFC) for the pyramid and detail how the unique challenges on the element and forest level associated with the pyramidal refinement are resolved. We propose the necessary functional design and generalize the fundamental global parallel algorithms for refinement, coarsening, partitioning, and face ghost exchange to fully support this new element. Our demonstrations confirm the efficiency and scalability of this complete, hybrid-element dynamic AMR framework.

**Key words.** Adaptive mesh refinement, parallel algorithms, forest of octrees, hybrid mesh, pyramid

**AMS subject classifications.** 65M50, 68W10, 65Y05, 65D18

**1. Introduction.** Numerical simulations are indispensable for analyzing complex physical systems. The fidelity of their results depends critically on the spatial resolution of the simulation domain. Adaptive meshes are widely used for efficient resolution of local features, which reduces computational cost [1, 15, 30, 39]. The prevailing strategy for distributing the computational mesh onto multiple processes is graph-oriented partitioning [42, 47, 48, 50]. It typically relies on third-party libraries [5, 26, 27, 38] to compute near-optimal partitions that minimize inter-process communication. While these algorithms are well established for static unstructured meshes, where the partition is computed only once, their computational overhead becomes a significant factor in dynamic scenarios and for extreme process counts.

A robust alternative to graph-based partitioning is dynamic, hierarchical adaptation based on a forest of refinement trees. This approach exploits the locality-preserving properties of *space-filling curves* (SFCs) [18, 34, 37, 40, 41] to linearize the multidimensional domain. While classically restricted to quadrilateral or hexahedral elements [43], this method allows for rapid, logic-based repartitioning without the overhead of global graph algorithms. Consequently, it is highly effective for massively parallel, dynamic simulations, as demonstrated by several scalable implementations [11, 17, 46, 49], some of which are now integrated into general-purpose parallel-computing libraries [2, 10, 22].

Most of these libraries support the usage of a fixed element shape, such as pure hexahedral or pure tetrahedral meshes. Both choices come with their own strengths and weaknesses; for example, hexahedral elements are beneficial to various classes of

---

\*Universität zu Köln, Germany, and Institute of Software Technology, German Aerospace Center (DLR), Cologne, Germany ([david.knapp@dlr.de](mailto:david.knapp@dlr.de))

†Institute of Software Technology, DLR, Cologne, Germany ([johannes.holke@dlr.de](mailto:johannes.holke@dlr.de))

‡Institute of Software Technology, DLR, Cologne, Germany ([thomas.spenke@dlr.de](mailto:thomas.spenke@dlr.de))

§Institut für Numerische Simulation (INS) and Hausdorff Center for Mathematics (HCM), Rheinische Friedrich-Wilhelms-Universität Bonn, Germany

solvers, while tetrahedra offer more flexibility to cover complex geometries. Combining both shapes can be advantageous but requires bridging elements, such as prisms or pyramids, to prevent hanging edges [16,23]. By themselves, these shapes do not offer further advantages, but they allow for conforming transitions wherever tetrahedral and hexahedral mesh elements meet.

In this paper, we present a generalization of Morton-type space-filling curves [36] to pyramids, a crucial development that enables fully general, tree-based hybrid adaptive mesh refinement (AMR) [23,24]. In previous works, we have established the underlying theory, parallel algorithms, and scalable demonstrations for hypercubical and simplicial elements up to three dimensions [8], and we have conducted initial research on suitable space-filling curves for prisms [31] and pyramids [32]. To fully support the pyramid primitive in practice, this work introduces a set of new per-element algorithms, such as computing the child, parent, and face neighbor, along with extensions to global mesh modification and interrogation algorithms like computing the bounds of a uniformly partitioned mesh. We present a reference implementation within the open-source adaptive-meshing software library `t8code` [20].

We propose a novel refinement strategy that partitions a pyramid into six pyramidal and four tetrahedral children. The decisive advantage of this decomposition is its commutativity with cubic refinement. Analogous to the tetrahedral Morton index [19], this property allows us to uniquely identify any pyramid in the forest solely by its enclosing sub-cube and a local orientation integer. Unlike standard element shapes that refine self-similarly, this strategy results in heterogeneous children (pyramids and tetrahedra). While this geometric irregularity poses a significant challenge for low-level index arithmetic, our solution overcomes this barrier, providing the essential component to enable fully general, tree-based hybrid adaptive mesh refinement.

**1.1. Summary.** Our proposed refinement strategy introduces heterogeneity in the descendants, as children of a pyramid are either tetrahedra or pyramids. Furthermore, the refinement pattern leads to a structure that is neither strictly self-similar nor uniformly balanced, with child numbers of eight (for tetrahedra) or ten (for pyramids). This geometric complexity requires sophisticated, novel approaches for the atomic element algorithms. For example, generating a sibling element, which is a straightforward operation for hypercubes and manageable for simplices, becomes non-trivial due to the mixed nature of the children. We propose functional designs for these essential algorithms and describe how the fundamental global parallel routines for refinement, coarsening, and gathering ghost elements are successfully generalized to robustly include pyramids.

The design of the space-filling curve itself is achieved through a relatively benign generalization, following the successful methodology developed previously for tetrahedra. Crucially, primitives like six tetrahedra, two prisms, or the combination of two pyramids and two tetrahedra (as shown in Figure 3.1c) may be arranged to tile a reference cube. We complement the standard cubic Morton SFC by introducing a type index that uniquely counts through the multiple, similar incarnations of a given primitive within that reference cube.

The partitioning algorithm follows without additional efforts, since it relies entirely on the SFC. The adaptive refinement and coarsening, however, are complicated significantly by several novel aspects:

1. Each pyramid refines into six pyramids and four tetrahedra; each of the pyramids may have one of two orientations in relation to the reference cube. This makes the generation of an initial uniform mesh non-trivial, since it contains

- a mix of equal-depth pyramidal and tetrahedral elements.
2. Formally generating the parent within pyramid refinement trees is quite involved compared to the much simpler algorithms for hexahedra, tetrahedra, and prisms, since it is not obvious whether the parent of a tetrahedron is a tetrahedron or a pyramid.
  3. The face neighbor of a pyramid may be taken across a triangular or a quadrilateral face, as opposed to standard element shapes in `t8code` like tetrahedra and hexahedra, for which the face always has the same shape. This requires additional lookup tables and branching.

Section 2 briefly reviews the forest-of-octrees structure implemented in `t8code`. We define and encode the space-filling curve for pyramids in Section 3. Section 4 develops the necessary per-element algorithms. In Section 5, we describe the global parallel algorithms for mesh manipulation, including the generation of the initial hybrid forest. We conclude in Section 6 and Section 7 with demonstrations of the efficiency and scalability of this new, fully hybrid approach to dynamic AMR.

**2. `t8code` and its parallel view of the forest.** The open-source software `t8code` [20] is our reference implementation of parallel, hybrid, dynamic, adaptive mesh refinement via a suite of dedicated parallel algorithms. The word *parallel* refers to the distributed storage of mesh data and metadata as well as its modification via concurrent algorithms that communicate over MPI [35]. With *hybrid* we refer to mixing elements of different primitive shapes in the same mesh, and *dynamic* refers to generating and modifying a parallel mesh in-core during a simulation at negligible cost compared to the overall runtime. Presently, and not barring future extension, it encodes topological neighbors across mesh faces. Thus, `t8code` addresses a subset of the full face, edge, and corner connectivity supported by the `p4est` software [6]. `p4est`, on the other hand, is focused strictly on quadrilateral and hexahedral elements and offers no route towards the hybrid refinement native to `t8code`.

`t8code` [8], like `p4est` [11] and `deal.II` [3] before, uses an unstructured mesh as a starting point for its operations, the so-called *coarse mesh*, which is usually given as the output of a mesh generator. Every element in this coarse mesh corresponds to one tree in the overall data structure, known as the *forest* made of these trees. The coarse mesh of `t8code` encodes the shape of its root elements and the connection to a neighboring tree for each of its faces not on the domain boundary. Adaptively refining the trees, we create a distributed set of *leaves* that become the elements of the refined mesh. The space-filling curve induces a consecutive index over the leaf elements, which enables simple and efficient load balancing across multiple processes. Storing only the leaves of the tree, decidedly ignoring all interior tree nodes, has been pioneered with the `dendro` code [44] and is often called *linear* octree storage. This concept enables supremely efficient data handling and evolves from the first generation of distributed octree codes [46].

As illustrated in Figure 2.1, each process holds its local elements and may also store its neighboring elements on other processes, which we call *ghost* elements. In 3D, `t8code` currently supports hexahedral, tetrahedral and prism elements using space filling curves. However, a suitable space-filling curve for pyramids did not exist so far. We address this gap by introducing a novel curve in this work.

**3. A pyramidal refinement and space-filling curve.** In this section we introduce the mathematical concept of a hierarchical pyramidal refinement and define the space-filling curve it induces. The anchor of our construction is the root pyramid, for which we specify a refinement scheme that defines its children. Following the

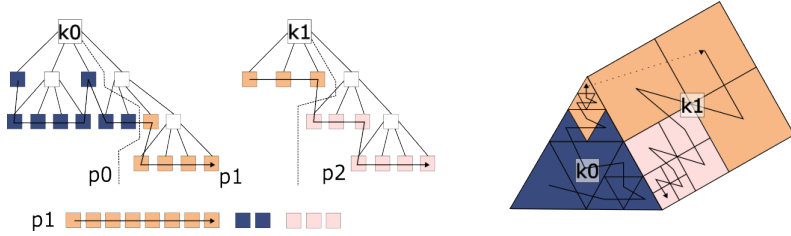


Fig. 2.1: The forest-of-trees approach used in `t8code`. The trees  $k_0$  and  $k_1$  are uniformly partitioned over three processes  $p_0, p_1, p_2$ . Each process holds its local elements and the ghost elements. The black arrow indicates the order of the elements by the space-filling curve index. The array of elements shows the elements stored by  $p_1$ .

construction of children of other elements, i.e., cutting the corners of the element, we get pyramidal children in the corners of a pyramid and tetrahedra in between; see Figure 3.1a and Figure 3.1b.

Upon further refinement, the tetrahedra resulting from the pyramidal decomposition will refine self-similarly, meaning they yield only tetrahedral children. For this, we can directly reuse published concepts, definitions, and algorithms based on Bey’s refinement scheme [4, 8]. A reference cube is split into six similar tetrahedra such that any descendant tetrahedron is a scaled version of one of the original six. When the Morton space-filling curve [36, 45] is applied to the refinement of the initial cube, each descending cube partitions into six tetrahedral descendants at the same refinement level, or depth. This ensures that cubic and tetrahedral refinement commute. This commutativity allows us to uniquely identify each tetrahedral descendant using a concise index tuple: its level, the coordinates of the surrounding cube descendant’s lower-left-back corner (*anchor coordinate*), and its type  $\in \{0, \dots, 5\}$ . The type encodes the specific orientation of the element within its enclosing sub-cube.

For the pyramidal children, a novel refinement strategy is required. Existing solutions for pyramidal subdivision often result in an undesirably large number of element types or introduce entirely new element shapes [25, 28, 29], which significantly increases the complexity of adaptive mesh refinement algorithms. Our design goal is a refinement that avoids producing degenerate mesh elements, maintains a minimal number of element types, and commutes with cubic refinement. A naive extension of Bey’s refinement to pyramids would typically involve dividing the root cube into three similar pyramids rotated 120 degree along a long diagonal. However, recursively applying this subdivision scheme quickly increases the number of distinct child shapes, leading to significantly more complex indexing and low-level algorithms.

To fulfill our requirements we propose a novel decomposition of the reference cube. We place two pyramidal elements within the cube, where one is a 180-degree rotation of the other, leaving two tetrahedral gaps. This arrangement guarantees that every pyramidal descendant is a scaled version of one of the original two. Furthermore, this decomposition allows us to leverage and reuse existing, established algorithms for the tetrahedral children of a pyramid, significantly reducing the overall algorithmic complexity.

Thanks to this strategy, pyramidal and cubic refinement commute, and we can define each pyramid by its surrounding descendant cube and its type  $\in \{6, 7\}$ . With this convention, the shape of any descendant of the root pyramid is implicit in its type. In analogy to tetrahedral elements, we therefore uniquely define a pyramid by

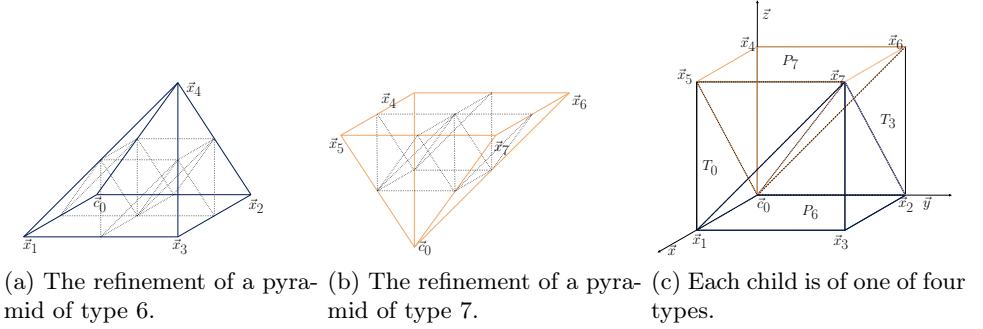


Fig. 3.1: (a): The vertices of a pyramid of type 6 and its ten children. The vertex  $\vec{c}_0$  is the anchor coordinate of the parent. The pyramid refines into six pyramids, one of them upside down, and four tetrahedra of two types. (b): The vertices of a pyramid of type 7 and its ten children. (c): the two different types of the pyramids and the tetrahedra, respectively, that occur as children, partition the cube. Defining the refinement this way, the cube (c) is also a sub-cube of (a) and (b). Note that both types of pyramids share the same anchor coordinate. Only the pyramid in the middle switches the type, that is the center pyramid of (a) is a pyramid of type 7 and the center pyramid of (b) is a pyramid of type 6.

Child	0	1	2	3	4	5	6	7	8	9
Parent of type 6	0	$\vec{h}_x$	$\vec{h}_x$	$\vec{h}_y$	$\vec{h}_y$	$\vec{h}_{xy}$	$\vec{h}_{xy}$	$\vec{h}_{xy}$	$\vec{h}_{xy}$	$\vec{h}_{xyz}$
Parent of type 7	0	$\vec{h}_z$	$\vec{h}_z$	$\vec{h}_z$	$\vec{h}_z$	$\vec{h}_{xz}$	$\vec{h}_{xz}$	$\vec{h}_{yz}$	$\vec{h}_{yz}$	$\vec{h}_{xyz}$

Table 3.1: This table defines how to shift the anchor coordinate of a pyramid of type 6 or 7 to compute the anchor coordinate of one of its children.  $\vec{h}_{\{\text{axes}\}}$  refers to a shift along all the given axes for a pyramid of length  $h$ , yet to be divided by two.

its *anchor coordinate*  $\vec{c}_0$  (see Figure 3.1c), its level, and its type.

Upon refinement, we divide a pyramid into ten children: six pyramids and four tetrahedra, as displayed in Figure 3.1. Each child can be identified by a shift of its parent’s anchor coordinate (see Table 3.1) and its type, which also depends on that of the parent (see Table 3.2).

The original pyramid, which has no parent, has level 0 and is called the *root pyramid*  $P^0$ . For practical purposes, we map the root pyramid into a reference cube of length  $2^\mathcal{L}$ , see pyramid  $P_6$  in Figure 3.1c. Therefore, every element’s anchor has integer coordinates up to the maximal level  $\mathcal{L}$ . Altogether we define the set of elements in a pyramidal refinement tree as follows:

DEFINITION 3.1.  $\mathcal{P} := \{P \mid P \text{ is a descendant of } P^0, \text{ with } 0 \leq l(P) \leq \mathcal{L}\}$ .

Similar to other elements, the pyramidal space-filling curve uses the interleaving of the coordinates and the type of the pyramid. Whenever we are talking about the coordinates we refer to their binary representation with  $\mathcal{L}$  bits. Additionally, we use  $X$ ,  $Y$ , and  $Z$  to denote the respective parts of the anchor coordinate of an element.

As outlined above, we inherit six types (0 to 5) for the tetrahedral children and add the types 6 and 7 for the pyramidal children (see Figure 3.1c). We define  $P^i$  as

Child	0	1	2	3	4	5	6	7	8	9
Parent of type 6	6	3	6	0	6	0	3	6	7	6
Parent of type 7	7	0	3	6	7	3	7	0	7	7

Table 3.2: The type for every child of a pyramid of type 6 and 7. In each sub-cube we order the elements by its type. Therefore, the tetrahedral children (types 0 to 5) in a sub-cube are the predecessors of the pyramidal children (types 6 and 7).

the  $i$ -th descendant along a branch towards an element  $P$ . Furthermore we split the type of an element in the pyramidal refinement tree into three tuples.

DEFINITION 3.2. *Let  $P \in \mathcal{P}$  be an element of level  $l$ .  $B(P)$  is defined as the  $\mathcal{L}$ -tuple consisting of the types of  $P$ 's ancestors in the first  $l$  entries, starting with the root pyramid  $P^0$ . The last  $\mathcal{L} - l$  entries of  $B(P)$  are zero:*

$$(3.1) \quad \begin{aligned} B = B(P) &= (\text{type}(P^1), \text{type}(P^2), \dots, \text{type}(P), 0, \dots, 0) \\ &= (b_{\mathcal{L}-1}, \dots, b_0) \in \{0, \dots, 7\}^{\mathcal{L}}, \end{aligned}$$

where the entry  $b_i$  is given by:

$$(3.2) \quad b_i = \begin{cases} \text{type}(P^{\mathcal{L}-i}), & \mathcal{L} - 1 \geq i \geq \mathcal{L} - l, \\ 0, & \mathcal{L} - l > i \geq 0. \end{cases}$$

In the refinement tree of a pyramid we find eight different types of elements, that is, two pyramidal and six tetrahedral shapes. Therefore, we can rewrite each entry  $b_j$  as a 3-digit binary number  $b_j = (b_j^2, b_j^1, b_j^0)_2$ . This gives rise to three new  $\mathcal{L}$ -tuples  $B^2, B^1$  and  $B^0$  with

$$(3.3) \quad \begin{aligned} B^0 &= (b_{\mathcal{L}-1}^0, \dots, b_0^0), \\ B^1 &= (b_{\mathcal{L}-1}^1, \dots, b_0^1), \\ B^2 &= (b_{\mathcal{L}-1}^2, \dots, b_0^2). \end{aligned}$$

Eventually, we define the *pyramid index* as the bit-wise interleaving of these tuples, concatenating the first bit of each in turn, then the second of each, etc.:

DEFINITION 3.3. *The pyramid index of an element  $P \in \mathcal{P}$  is given as the interleaving of the  $\mathcal{L}$ -tuples  $Z, Y, X, B^2, B^1$ , and  $B^0$ , written*

$$(3.4) \quad m_P(P) := Z \dot{\downarrow} Y \dot{\downarrow} X \dot{\downarrow} B^2 \dot{\downarrow} B^1 \dot{\downarrow} B^0.$$

Consequently, for the same anchor node, the elements are ordered by their type. Hence, a type-0 tetrahedra comes before a tetrahedra of type 3, followed by the pyramids of type 6 and type 7; cf. Figure 3.1c.

In summary, we can uniquely identify an element in the pyramidal refinement using its pyramid index and its level. In effect, we construct the pyramid index such that we are able to prove that it is an SFC index according to the following definition from [19]:

DEFINITION 3.4. *Suppose we have a set of  $\mathcal{S}$  elements in the refinement of a pyramid. An SFC index  $\mathcal{I}$  is a map  $\mathcal{I} : \mathcal{S} \rightarrow \mathbb{N}_0$  with the following properties:*

1. Restricted to a level  $l$ ,  $\mathcal{I}$  is injective:  $\mathcal{I} \times l : \mathcal{S} \rightarrow \mathbb{N}_0 \times \mathbb{N}_0$  is injective.
2. If  $E$  is an ancestor of  $E'$  then  $\mathcal{I}(E) \leq \mathcal{I}(E')$  (refining is monotonous).
3.  $\mathcal{I}(E) < \mathcal{I}(\hat{E})$  and  $\hat{E}$  not a descendant of  $E$ , then  $\mathcal{I}(E) \leq \mathcal{I}(E') < \mathcal{I}(\hat{E})$  for all descendants  $E'$  of  $E$  (refining is local).

We show these three properties by embedding the pyramid index into a six-dimensional Morton index.

**THEOREM 3.5.** *The pyramid index  $m_P$  is an SFC index.*

We reduce the proof to the fact that the Morton index in any dimension is formally an SFC index [8]. Thus, we identify the anchor coordinates with the first three coordinates of the anchor node of the cube, and we map the three type-representing tuples  $B^0$ ,  $B^1$ , and  $B^2$  onto the last three coordinates of the anchor node. Since  $0 \leq B^i < 2^\mathcal{L}$ , we can use the set of children  $Q_0 := [0, 2^\mathcal{L}]^6$  to embed the pyramids.

Given the anchor node of a cube and its level, the set  $\mathcal{Q}$  of all six-dimensional cubes in the refinement is given as  $\mathcal{Q} = Q_{(x_0, \dots, x_5), l}$ , with  $x_0, \dots, x_5$  as the coordinates of the anchor node. The Morton index for six-dimensional cubes is given by the bit-wise interleaving of the coordinates of the cube as a generalization of the well-known 2D and 3D indices [36, 45]:

$$(3.5) \quad m_Q(Q) = X^5 \dot{\downarrow} X^4 \dot{\downarrow} X^3 \dot{\downarrow} X^2 \dot{\downarrow} X^1 \dot{\downarrow} X^0.$$

We use Proposition 3.6 to map the pyramid index to six-dimensional cubes.

**PROPOSITION 3.6.** *The map*

$$(3.6) \quad \begin{aligned} \Theta : \mathcal{P} &\rightarrow \mathcal{Q}, \\ P &\mapsto Q_{(B^2(P), B^1(P), B^0(P), x(P), y(P), z(P)), l(P))} \end{aligned}$$

*is injective and satisfies*

$$(3.7) \quad m_Q(\Theta(P)) = m_P(P).$$

*Furthermore, it ensures the property that  $P'$  is a child of  $P$  if and only if  $\Theta(P')$  is a child of  $\Theta(P)$ .*

*Proof of Proposition 3.6.* The equation  $m_P(P) = m_Q(\Theta(P))$  follows from the definition of the indices on  $\mathcal{P}$  and  $\mathcal{Q}$ . Using that an element is uniquely determined by its index and its level, we see that  $\Theta$  is injective. To show the second property, let  $P, P' \in \mathcal{P}$ , where  $P'$  is a child of  $P$ . Additionally let  $l = l(P)$ . We use that  $Q' := \Theta(P')$  is a child of  $Q := \Theta(P)$  if and only if for each  $i \in \{0, \dots, 5\}$  it holds that

$$(3.8) \quad x_i(Q') \in \left\{ x_i(Q), x_i(Q) + 2^{\mathcal{L}-(l+1)} \right\}.$$

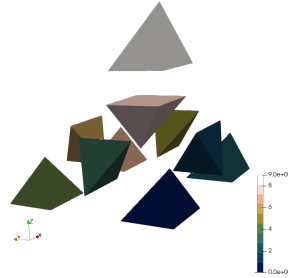
We know that (3.8) holds for the  $x$ -,  $y$ -, and  $z$ -coordinate of the anchor node of  $P'$ , meaning it holds for  $i \in \{3, 4, 5\}$ . By definition  $B^j(P')$  is the same as  $B^j(P)$  except for the new type at position  $\mathcal{L} - (l + 1)$ , for which

$$(3.9) \quad \begin{aligned} B^j(P')_{\mathcal{L}-(l+1)} &= b_{\mathcal{L}-(l+1)}^j(P') \in \{0, 1\} \quad \text{and} \\ B^j(P)_{\mathcal{L}-(l+1)} &= 0. \end{aligned}$$

In conclusion, (3.8) holds for  $i \in \{0, 1, 2\}$ , and the first implication is shown.

For the reverse implication we assume that  $\Theta(P')$  is a child of  $\Theta(P)$ . Since the level of  $P'$  is bigger than 0, we know that  $l(\Theta(P')) > 0$  and  $P'$  has a parent  $S$ . By the uniqueness of the parent of a cube the identity  $\Theta(S) = \Theta(P)$  must hold. Thus, we obtain  $S = P$ , since  $\Theta$  is injective and  $P'$  is the child of  $P$ .  $\square$

Fig. 3.2: A single pyramid that is refined once. Each child is colored according to its index. The element with the index 0 is colored red, the last element is colored blue.



Child	$P_0$	$T_1$	$P_2$	$T_3$	$P_4$	$T_5$	$T_6$	$P_7$	$P_8$	$P_9$
Parent of type 6	0	1	2	3	4	5	6	7	8	9
Parent of type 7	8	6	3	9	7	1	2	5	4	0

Table 3.3: The local index for every child of a pyramid of type 6 is consecutive by construction, while the order is non-trivial for a parent of type 7.

On this basis, we proceed to prove Theorem 3.5.

*Proof of Theorem 3.5.* The first two properties of an SFC index can be deduced by the fact that the Morton index for six-dimensional cubes is an SFC index together with Proposition 3.6. Using the last property of Proposition 3.6 inductively, we use that  $P'$  is a descendant of  $P$  if and only if  $\Theta(P')$  is a descendant of  $\Theta(P)$  to guarantee the third property of an SFC index.  $\square$

With the help of Figure 3.2 we define a *local index* of an element. The local index  $i$  refers to the  $i$ -th child of an element according to the SFC index. For a parent of type 6 the children are already ordered by the SFC, while the local index for parents of type 7 is not straightforward; see Table 3.3. Lastly, we observe the following two Lemmata by analyzing the refinement of a pyramid (see Figure 3.2) and the refinement of type 0 or 3 tetrahedra, which are the only tetrahedral children of a pyramid.

LEMMA 3.7. *The five pyramidal children touching a face of their parent lie in a corner of their parent.*

LEMMA 3.8. *A descendant of a tetrahedron in a pyramidal refinement tree that has a pyramid as a neighbor lies in a corner of its parent.*

A visualization of both lemmata can be seen in Figure 3.3.

**4. Algorithms at the element level.** In this section we give an introduction into the element-wise (low-level) algorithms for pyramids with a focus on the differences to the corresponding algorithms for other element shapes. Major differences for pyramids take effect when constructing the parent, as discussed in Section 4.1. Section 4.2 is a brief example of a typical low-level algorithm, namely constructing the child element of a given index. We proceed constructing neighboring elements inside the same pyramidal tree in Section 4.3. Neighbor elements across trees implicate a transformation and possibly a translation into a different shape, which we cover in Section 4.4.

**4.1. Parent.** For an element  $E$ , we can compute the ancestor of level  $l(E) - 1$  using the `parent` algorithm. Given the type of  $E$  and its anchor coordinate, we can

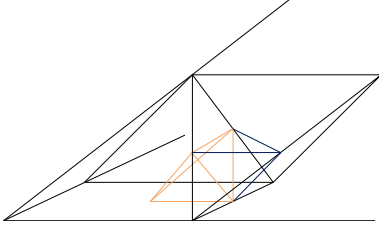


Fig. 3.3: A pyramid and its neighbor along  $f_3$ . In the refinement of the black (outer) pyramid, all children that do not have type 3 or 0 only have tetrahedral neighbors within the same tree.

compute the type of the parent. The level and the coordinates of the parent are given implicitly, by setting the  $l(E)$ -th bit of  $E$ 's coordinate to zero. We refer to this operation as “cutting”, especially when multiple bits of the coordinate are set to zero.

For a tetrahedron  $T$  descending from a pyramidal root element, the computation of the type is not trivial. In contrast to a pure tetrahedral tree (or other trees containing only one element shape), we cannot determine the type of the parent without further analysis.

One remedy would be to recompute the  $\mathcal{L}$ -tuple  $B$  (see Def. 3.2), descending from the root pyramid down to level  $l(E) - 1$ , to check at which level the last pyramidal ancestor of the tetrahedron occurs. This, however, is a rather costly computation; to avoid it, we introduce the field `min_tet_level`: For each element, it stores the smallest level at which the ancestor has the shape of a tetrahedron. We can compute this field during the construction of an element without using the iterative computation of the types of all ancestors. For all pyramids we set `min_tet_level` =  $-1$ , since they do not have any tetrahedral ancestor at all.

For a tetrahedron with a pyramidal parent, the type of the parent can be determined by comparing the  $z$ -coordinates:

- If the tetrahedron has the same  $z$ -coordinate as the anchor coordinate of the parent, the parent has type 6.
- Otherwise, the parent has type 7.

Aside from this computation of the type of the parent, the `parent` algorithm does not change for elements in a pyramidal refinement, see Algorithm 4.1.

**4.2. Child.** The child algorithm computes the  $i$ -th child of an input element  $E$ , with  $0 \leq i < N_c$ , where  $N_c$  denotes the maximal number of children of  $E$ . We can subdivide the problem into two cases:

- (a) If  $E$  is a pyramid, we shift the anchor coordinate based on the type of the input element by 0 or  $2^{\mathcal{L}-(l+1)}$ , with  $l = l(E)$ . Using the type of  $E$  and the local id  $i$ , we can determine the type of the child. Altogether, we can determine the child using the computed coordinates, the type, and the implicitly given level.
- (b) If  $E$  is a tetrahedron descending from a pyramid, we can reuse the algorithm implemented for tetrahedra, since the types of pyramids and tetrahedra do not interfere. Furthermore, the computation of the anchor coordinate is the same for pyramids and tetrahedra.

We use Tables 3.1 and 3.2 to look up these values for pyramids, see Algorithm 4.2.

**4.3. Same-tree neighbor elements.** This section describes how to compute the neighbors of an element inside of a tree. In Section 4.4 we describe the computation of neighbors over tree boundaries. The computation of ghost elements for one process requires the computation of an element's neighbor along a given face. We divide the problem into three sub-tasks and solve them subsequently:

1. Define the shape of the neighbor. The neighbor of a pyramid may be another

**Algorithm: t8\_dpyra\_parent**

**Data:** An element  $E$  and an empty element  $P$ , which is going to be filled with the data of the parent of  $E$ .

```

P.level = E.level - 1                                ▷Set level of parent P
if  $E$  is a pyramid then
  Note: P is a pyramid
   $c_{id} = \text{cube\_id}(E, E.\text{level})$                 ▷Compute the cube id of E
   $P.\text{type} = \text{from}(E.\text{type}, c_{id})$                 ▷Determine type of P
   $P.\text{coord} = \text{cut}(E.\text{coord})$                     ▷Set P's coordinates via cutting
   $P.\text{min\_tet\_level} = -1$                         ▷Set min_tet_level to invalid
else
  if  $E.\text{min\_tet\_level} = E.\text{level}$  then
    Note: P is a pyramid
     $P.\text{type} = \text{from}(E.\text{coord})$                 ▷Determine type of P
     $P.\text{coord} = \text{cut}(E.\text{coord})$                     ▷Set P's coordinates via cutting
     $P.\text{min\_tet\_level} = -1$                         ▷Set min_tet_level to invalid
  else
    Note: P is a tetrahedron
     $P = \text{tet\_parent}(E)$                             ▷Compute P as tetrahedral parent
     $P.\text{min\_tet\_level} = E.\text{min\_tet\_level}$         ▷Set lowest-level tetrahedral ancestor
  end
end

```

**Algorithm 4.1:** The algorithm to compute the parent of an element. To avoid the recomputation of the types of all ancestors, we introduce a new field `min_tet_level` that can be used to look up the smallest level at which an element's ancestor is a tetrahedron.

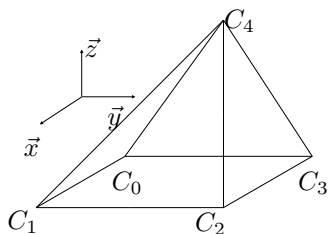


Fig. 4.1: The corners of a pyramid.

Face	corners			
$f_0$	$C_0$	$C_3$	$C_4$	–
$f_1$	$C_1$	$C_2$	$C_4$	–
$f_2$	$C_0$	$C_1$	$C_4$	–
$f_3$	$C_2$	$C_3$	$C_4$	–
$f_4$	$C_0$	$C_1$	$C_2$	$C_3$

Table 4.1: The faces of a pyramid.

pyramid or a tetrahedron; analogously, a tetrahedron's neighbor may either be another tetrahedron or a pyramid.

2. Compute the coordinates and the type of the neighbor.
3. Define the number of the dual face, i.e., the face of the neighbor touching the original element.

In order to identify the element's faces, we define a numbering of the corners and the faces of a pyramid. To be consistent with previous work, we choose the labels given in [9]; see Figure 4.1. We use  $f_i$  to denote the  $i$ -th face of an element, or  $f$  for a face in general. We use  $C$  to address a corner and  $C_i$  for the  $i$ -th corner. Note that we only define the numbering on a type-6 pyramid, because a pyramid of type 7 can be seen as a 180-degree rotation of a type-6 pyramid.

**Algorithm: t8\_dpyra\_child**

**Data:** An element  $E$ , a local index  $i$ , and an empty element  $C$ , which is going to be filled with the data of the  $i$ -th child of  $E$ .

```

C.level = E.level + 1           ▷ Set level of the child C
if  $E$  is a pyramid then
    |  $C.coord = E.coord + \text{shift}(i)$            ▷ Shift the coordinates using Table 3.1
    |  $C.type = \text{child\_type}(E.type, i)$        ▷ Set the type using Table 3.2
    | if  $C$  is a tetrahedron then
    | |  $C.min\_tet\_level = C.level$            ▷ Set min_tet_level
    | | end
else
    | Note:  $E$  is a tetrahedron
    |  $C = \text{t8\_tet\_child}(E, i)$              ▷ Call the tetrahedral routine
    |  $C.min\_tet\_level = E.level$            ▷ min_tet_level is the same for the child
end

```

**Algorithm 4.2:** The algorithm to compute the  $i$ -th child of an element. We use the Tables 3.1 and 3.2 for the computation of the anchor coordinate and the type of the child.

Local id	pyramid 6	pyramid 7	Face	$CTF_0$	$CTF_1$	$CTF_2$
1	1	3	$f_0$	1	2	3
2	–	3	$f_1$	0	2	3
3	1	–	$f_2$	0	1	3
5	0	2	$f_3$	0	1	2
6	0	–				
7	–	2				

(a) The faces of a tetrahedron inside a pyramid which extrude to a tetrahedron.

(b) The types of the three children touching a given face of a tetrahedron.

Table 4.2: The face connectivity between pyramids and tetrahedra.

**Shape of the neighbor.** In the following, we show how to determine the shape of the same-tree neighbor. For a pyramid, the quadrilateral face  $f_4$  is connected to another pyramid, while all other neighbors are always tetrahedra. Note that the tetrahedral children of a refined pyramid always have type 0 or 3, so only these can have a pyramid as a same-tree (and same-level) neighbor. Therefore, we can use the already existing algorithms for all tetrahedra that do not have type 0 or 3; see [8].

For a tetrahedron of type 0 or 3, we distinguish two cases when identifying the neighbor’s shape:

- (a) The parent of the tetrahedron is a pyramid. In that case, the tetrahedron has three faces touching its pyramidal siblings and one face connected to another tetrahedron. This face’s number depends on the type of the pyramidal parent and the local id of the element itself; it is defined in Table 4.2a.
- (b) The parent of the tetrahedron is another tetrahedron. It may have many tetrahedral ancestors, the most interesting being the tetrahedral ancestor with the lowest level, because its parent is a pyramid. If the input element touches a face of this lowest-level tetrahedral ancestor, we can reduce this case to the first case.

In conclusion, for both cases we need to know which face of a tetrahedron is touching

a pyramid and which one is not. The distinction is simplified by introducing the following definition of *valid faces*:

**DEFINITION 4.1.** *Let  $f$  be a face of a tetrahedron with pyramidal parent; if  $f$  is connected to a pyramid, it is called a valid face.*

It is important to realize that the problem of determining the shape of a tetrahedron's neighbor is not solved yet. In the above case (b), knowing an element is connected to a valid face is not sufficient to determine the shape of the neighbor. To derive the necessary additional checks, we observe that for a type-3 tetrahedron refined multiple times, the type of the children not in their parent's corner alternates between 2 and 3; since a type-2 tetrahedron can never touch a pyramid, this implies that only the children in the corner can have a pyramid as a neighbor.

Therefore, we check whether all ancestors up to the lowest-level tetrahedral ancestor are a child in the corner of their parent. If so, it follows that these ancestors and the element have the same type and the same face numbering, because the children at the corner always have the same type as their parents; see [8]. Hence, we have to check whether the given face of the ancestor is valid to determine the shape of the neighbor of the input tetrahedron. Now these arguments combine into the following theorem.

**THEOREM 4.2.** *Let  $T$  be a tetrahedron of type 0 or type 3 that has a pyramid as an ancestor,  $A = \arg \min_l \{S.l : S \text{ tetrahedron and ancestor of } T\}$  its lowest-level tetrahedral ancestor, and  $T' \in \{S \text{ ancestor of } T : S.l \geq A.l\}$  any tetrahedral ancestor of  $T$ ; then  $T$  has a pyramid neighbor along face  $f$  if and only if:*

- (i)  $T$  and all  $T'$  are in a corner of their parent touching face  $f$  of the parent, and
- (ii) face  $f$  of  $A$  is a valid face of  $A$ .

*Proof of theorem 4.2.* First, assume that there is a  $T'$  not touching the face  $f$  of its parent. Then no child of  $T'$  can have contact with this face again, so  $T$  does not touch face  $f$  of  $A$ . As a result,  $T$  cannot have a neighbor outside of  $A$ , meaning its neighbor has to be a tetrahedron, which is a contradiction. Secondly, assume that there is a  $T$  touching face  $f$  but not lying in the corner of its parent.  $T$  has an ancestor in the shape of a tetrahedron and since all children are tetrahedra, the neighbor of  $T$  is a tetrahedron which is a contradiction to Lemma 3.8. Eventually assume that the face  $f$  of  $A$  is not a valid face. But then, the neighbor along this face can not be a pyramid by the definition of a valid face, see Definition 4.1.

For the other direction we assume that  $T$  does not have a pyramid neighbor along face  $f$ . Therefore the neighbor is a tetrahedron. If its parent is a pyramid, the tetrahedron cannot lie in the corner of the pyramid (by Lemma 3.7). Using this argument recursively we see that there is either a  $T'$  not lying in the corner of its parent, or there is a  $T'$  in the corner opposite of  $f$ , hence not touching it. Furthermore,  $f$  has to be a valid face by the definition of it.  $\square$

We can identify the children of a tetrahedron touching a given face by their local indices, see Table 3.3. Since the face number of a tetrahedron is given by the number of the opposite corner, we can use Table 4.2b to check whether a child is touching a given face. For every tetrahedral ancestor, we check the local index: if it always refers to the same corner, the neighbor might be a pyramid. The complexity of this check grows linearly with the level. To avoid it as often as possible, we first check if the given face is a valid face, which can be done in constant time via the position of the tetrahedron in its pyramidal parent, using Table 4.2a. At this point we have solved the first problem and provide Algorithm 4.3 to determine for an element of type 0 or

3 whether the neighbor along the given face is a pyramid.

**Algorithm: t8\_dtet\_pyra\_touch**

**Data:** An element  $T$  of type 0 or type 3 and a face number  $f$

```

if  $T.level = T.min\_tet\_level$  then
  | return  $tet\_pyra\_connect(T, f)$       ▷ Use type check of Table 4.8
end
 $A = tet\_anc(T, T.min\_tet\_level)$       ▷ Get lowest-level tetrahedral ancestor
 $valid = tet\_pyra\_touches\_face(A, f)$   ▷ Check if  $A$  touches  $f$ 
if  $valid$  then
  | Note: If all ancestors of  $T$  until  $A$  touch  $f$ , then  $T$  touches  $f$ 
  |  $type = T.type$                         ▷ Start tests with  $T$ 
  | for  $l = T.level; l > A.level; l--$  do
  |   |  $c_{id} = cube\_id(T, l)$              ▷ Compute the cube id on level  $l$ 
  |   |  $id = cube\_id\_to\_Beyes(type, c_{id})$  ▷ Get the local id
  |   | if not  $child\_touches\_face(f, id)$  then
  |   |   | return  $false$                 ▷ All children have to touch face  $f$ 
  |   |   end
  |   |  $type = parent\_type(c_{id}, type)$   ▷ Type might vary each level
  |   end
  | end
  | return  $valid$ 

```

**Algorithm 4.3:** The algorithm to decide for a tetrahedron of type 0 or 3 whether the neighbor along a face  $f$  of the root is a pyramid.

**Coordinates and type of the neighbor.** Next, we solve the second problem, i.e., computing the type and the anchor coordinate of the neighbor based on its shape. As above, the computation is separated into pyramidal and tetrahedral input elements.

In Table 4.3, the types and shapes of a pyramid's neighbors are given for each face, that is, tetrahedra of type 0 or 3 for the triangular faces  $f_0, f_1, f_2, f_3$  and the opposite pyramid for the quadrilateral  $f_4$ . To compute the coordinates of the neighbor, we consider two cases which can be organized in one table each:

- (a) For a pyramid, the differences of the neighbor's anchor coordinates compared to the pyramid itself are given in Table 4.4. It shows that for tetrahedral neighbors, only the  $x$ - and  $y$ -coordinates differ, while the  $z$ -coordinate is the same; for the pyramidal neighbor at face  $f_4$ , in contrast, only the  $z$ -coordinate changes.
- (b) For a tetrahedron with a pyramid as neighbor, the computation of the coordinates can be done in a similar fashion, see Table 4.5.

**Dual face number.** Eventually, we determine the number of the dual face. If the neighbor of a tetrahedron is a tetrahedron too, we use the already existing algorithm for tetrahedra. If the input element is a pyramid, the dual face number depends on the pyramid type and the given face number. Given the type of the input element and the face, the computation of the dual face can be done efficiently using Table 4.6.

If we run the costly check whether a tetrahedron has a pyramid neighbor last, we can avoid it as often as possible. All other checks run in constant time.

**4.4. Inter-tree neighbor elements.** This section addresses the computation of neighbors outside the root pyramid. We follow the strategy used in `t8code` to compute neighbors over the boundaries of a tree. It is based on the fact that two

Table 4.3: The type of the neighbor of a pyramid given a face of the pyramid and its type.

Face	pyramid 6	pyramid 7
$f_0$	3	3
$f_1$	3	3
$f_2$	0	0
$f_3$	0	0
$f_4$	7	6

Coordinate	$f_0$	$f_1$	$f_2$	$f_3$	$f_4$
$x$	0	len    0	0	0    -len	0
$y$	0	0    -len	0	len    0	0
$z$	0	0	0	0	-len    len

Table 4.4: The manipulation of the coordinate of a pyramid to compute the coordinates of the neighbor along a given face, with  $\text{len} = 2^{\mathcal{C}-l}$  the length of the face given its level  $l$ . For each coordinate, the entry in the table has to be added to the coordinate of the input pyramid. We abbreviate pairs of assignment:  $a \parallel b$  means that  $a$  is chosen if  $\text{type} = 6$  and  $b$  otherwise, i.e., meaning  $\text{type} = 7$ .

elements share a face planar with the tree boundary. This computation is split in two main parts:

1. Within the root pyramid, we have to be able to collapse an element to the face that touches the root's boundary.
2. On the other side, i.e., in the adjacent coarse-mesh element, we need the inverse of this process: Given a face on the boundary, we want to construct the associated element in the root pyramid.

Note that other elements in the forest may have different maximal levels, which has to be considered when computing the neighbor over the face of the root element. For the sake of simplicity, however, we neglect this additional computation here, as it only affects the scaling of the computed coordinates.

**Collapsing to a face.** In the following, we show how to collapse an element down to a given face, starting with a pyramid: For each face element, Table 4.7 lists its anchor coordinates and its type. While the anchor coordinate of the quadrilateral face matches that of the pyramid, those of the four triangular faces are obtained through a coordinate permutation. The coordinates need to be scaled to the correct maximal level.

Note that (unlike prisms, pyramids, tetrahedra, and triangles) quadrilateral elements do not have a type.

To instead collapse a tetrahedron within the root pyramid, we first have a look at the following example: Given a pyramid that is refined once, we see that its tetrahedral children are between two pyramids, and have type 0 or 3. Since the boundary surfaces of the pyramidal children have type 0, the boundary surfaces of a tetrahedral child have type 1. If we refine this tetrahedron again, another type of tetrahedron arises in the middle. If we refine further, we observe that the type of the tetrahedra in the middle of the face alternate between two different types. Depending on the given face, the new arising type is 2 or 1. These elements touch the root with a triangular face of type 0.

In conclusion, if the tetrahedron touching the root face has type 0 or 3, the triangle

Coordinate	$f_0$	$f_1$	$f_2$	$f_3$
$x$	(len    0)	0	0	(0    -len)
$y$	(0    len)	0	0	(-len    0)
$z$	0	0	0	0
Type	7	7	6	6

Table 4.5: The manipulation of the coordinate of a tetrahedron neighboring a pyramid along a given face. For each coordinate the entry at the table has to be added to the coordinate of the input pyramid. By  $(a || b)$ , we abbreviate the cases for type 0 ( $a$ ) or the other types ( $b$ ).

Type	$f_0$	$f_1$	$f_2$	$f_3$	$f_4$
0	$f_3$	$f_2$	$f_2$	$f_3$	—
3	$f_1$	$f_0$	$f_0$	$f_1$	—
6	$f_2$	$f_3$	$f_2$	$f_3$	$f_4$
7	$f_1$	$f_0$	$f_1$	$f_0$	$f_4$

Table 4.6: The (dual) face number of the neighbor of an element given the input type and a face.

has type 1, otherwise it has type 0, as listed in Table 4.8.

**Construct pyramid from face.** Next, we discuss the inverse operation: construct a volume element that touches a given surface element on a face of the root pyramid. Since tetrahedra have already been introduced in previous work, this section is restricted to constructing pyramidal elements.

Determining the pyramid’s anchor coordinate differs from face to face; Table 4.9 provides an overview.

- From a quadrilateral face element we can directly compute the pyramid. The anchor coordinates are given by those of the quadrilateral extended by a  $z$ -coordinate of zero; in the end, we scale the coordinates to the length of the root pyramid.
- For all triangular faces, the  $z$ -coordinate of the pyramid is given by the  $y$ -coordinate of the face; setting its  $x$ - and  $y$ -coordinates is only slightly more involved: as detailed in Table 4.9, they are either given directly from the face’s  $x$ - and  $y$ -coordinates or have to be computed as the difference in length between the root element and a pyramid of the same level as the triangle.

In addition to the anchor coordinates, we need to compute the type of the pyramid. We know for all triangles of type 1 that the extruded element is a tetrahedron of type 0 or type 3 (depending on the given root face). Accordingly, only if the triangle has type 0, we need to check whether the extruded element is a pyramid or a tetrahedron, see Figure 4.2 for an visualization of the extrusion of different triangles. The element that a type-0 face extrudes to is a tetrahedron if and only if it has a tetrahedron as a parent; otherwise, it is a pyramid. In Theorem 4.1, we show how to check the property on a binary level.

**THEOREM 4.3.** *Let  $T$  be a triangle of type 0 on the surface of the root pyramid. The boundary element with  $T$  as a face is a pyramid if and only if*

$$(4.1) \quad T \rightarrow y = T \rightarrow x \ \& \ T \rightarrow y,$$

with “&” referring to a bitwise AND.

Coordinate	$f_0$	$f_1$	$f_2$	$f_3$	$f_4$
$T.x$	$y$	$y$	$x$	$x$	$x$
$T.y$	$z$	$z$	$z$	$z$	$y$
Type	0	0	0	0	quad

Table 4.7: The coordinates and type of a face of pyramid  $P$  that touches the root element with a given face number of  $P$ . For the faces 0 to 3 the faces are triangles of type 0; for face 4, the face is a quadrilateral element, which does not have a type. The coordinates  $x$ ,  $y$ , and  $z$  refer to the coordinates of the input element.

(Type, face)	$(0, f_1), (2, f_2)$	$(0, f_0), (1, f_0)$	$(3, f_1), (1, f_2)$	else
$T.x$	$y$	$y$	$x$	$x$
$T.y$	$z$	$z$	$z$	$z$
Type of face	$(0 ? 1 \parallel 0)$	$(0 ? 1 \parallel 0)$	$(3 ? 1 \parallel 0)$	$(3 ? 1 \parallel 0)$

Table 4.8: The coordinates and type of a tetrahedron's face that touches the root element. Both depend on the face and type of the element. All boundary elements are triangles. We abbreviate the choice of type in the last row by  $(t ? a \parallel b)$ , where  $a$  applies to type  $t$  and  $b$  otherwise.

*Proof of Theorem 4.1.* Let  $T$  be a triangle of type 0 on the surface of the root pyramid that touches a pyramid as an inter-tree neighbor. As pyramids touching a face of its parent only occur in the corners, all the ancestors of  $T$  lie in a corner of their parent. The statement holds for triangles of level 0 and we use an inductive argument to show the first direction:

Assume it holds for the first  $l$  bits that  $T \rightarrow y = T \rightarrow x \& T \rightarrow y$ . In the corners of a triangle of type 0 are the children with local id 0, 2, and 3.

- The child with local id 0 does not change the coordinates.
- The child with local id 2 flips the  $(l + 1)$ -th bit to 1 for the  $x$ -coordinate, while the  $y$ -coordinate remains unchanged. Thus the equation still holds.
- For the child with local id 3, both the  $x$ - and the  $y$ -coordinate are flipped to 1 at the  $(l + 1)$ -th bit and the equation still holds.

Next, let  $T$  be a triangle of type 0 which fulfills the equation. Then every bit of the coordinates has to fulfill the equation. Each bit describes the position of a triangle in its parent. The combinations of bits of  $x$ - and  $y$ -coordinates fulfilling the equation are  $(0, 0)$ ,  $(1, 0)$ , and  $(1, 1)$ . The type-1 child of a triangle fulfills the equation too, but its type-0 child at the next level does not. Thus, at every bit the coordinates refer to a corner triangle. Therefore, the extruded element with face  $T$  has the shape of a pyramid.  $\square$

The type of the neighboring tetrahedron depends on the type of the triangle and the number of the root face and can be computed via a look up Table 4.10a. At last, we need to compute the number of the face of the pyramid touching the root face. If the shape is a pyramid, it is the number of the given root face. Otherwise it depends again on the type of the triangular element and the given root face, and can be computed via a look up Table 4.10b.

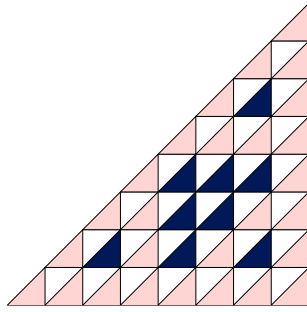


Fig. 4.2: A triangular face of a pyramid that has been refined 3 times. All white triangles have type 1 and we know directly that they are extruded to a tetrahedron. We marked all type 0 triangles that expand to a pyramid in light pink. All blue type 0 triangles extrude to a tetrahedron.

Coordinate	$f_0$	$f_1$	$f_2$	$f_3$	$f_4$
$P.x$	$y$	$2^L - 2^{T \rightarrow \text{level}}$	$x$	$x$	$x$
$P.y$	$x$	$x$	$y$	$2^L - 2^{T \rightarrow \text{level}}$	$y$
$P.z$	$y$	$y$	$y$	$y$	0

Table 4.9: The coordinates of an extruded element on the face of the root pyramid. We notice that on face 4 the elements are quadrilaterals, the elements on all other faces are triangles. We refer with  $x$  and  $y$  to the coordinates of the triangle  $T$  on the face of the root element.

**5. Algorithms at the forest level.** Global, high-level procedures for mesh manipulation, information gathering, or searching can be implemented independently of the element-specific routines. The forest-level view allows general processing and communication of mesh metadata by simply calling the necessary element-specific virtual functions. In Section 6 and Section 7, we will investigate how the pyramid-specific functions influence the performance and scalability of a set of exemplary forest-level algorithms:

- **New** creates a uniformly refined forest of a given depth that is partitioned equally over all available processes.
- **Adapt** evaluates a user-provided criterion to decide whether an element should be refined, stay as it is, or whether a family of elements should be coarsened into their parent element.
- **Partition** repartitions a forest; based on the number of elements in the mesh, the boundaries for each process are computed and the elements (and possible data connected to them) are communicated to reestablish an equal-weight partition over all processes.
- **Ghost** determines the remote face-neighbor elements of every process and gathers them in a symmetric point-to-point communication scheme.

When generating an initial forest, the first task is to compute a partitioned uniform mesh via **New**. This involves determining the assignment of coarse mesh elements (trees) based on a target refinement level, ensuring a balanced element count per process after the initial uniform refinement.

For standard isotropic refinement, the number of elements in a uniformly refined tree at level  $\ell$  is determined by the refinement factor (e.g.,  $N(\ell) = 2^{\text{dim} \cdot \ell}$ ). If all element types share the same refinement ratio, partitioning is straightforward, requiring only the total element count.

Type	$f_0$	$f_1$	$f_2$	$f_3$	Type	$f_0$	$f_1$	$f_2$	$f_3$
0	1	1	2	0	0	2	0	2	0
1	0	0	3	3	1	1	0	1	0

(a) The type of the tetrahedron touching the root pyramid, given a root face.

(b) The type of the constructed tetrahedron touching the root face.

Table 4.10: Relations between the faces of the root pyramid and tetrahedra.

However, the pyramid refinement introduced here transcends this simple assumption. Pyramidal descendants use different refinement factors (eight or ten), depending on whether they are a pyramid or tetrahedron, leading to the following element total for an  $\ell$ -times refined root pyramid,

$$(5.1) \quad N(\ell) = 2 \cdot 8^\ell - 6^\ell,$$

see [SM1](#) for a quick derivation. Furthermore, mixing pyramids with other element shapes means not all trees refine in the same manner. Consequently, achieving a fair initial load assignment requires a non-trivial algorithm, which we detail in [Section 5.1](#).

Considering future developments in adaptive refinement, a generalized methodology extending beyond the pyramidal case is beneficial for the `New` algorithm. This generality will support advanced techniques, such as the mixing of anisotropic and isotropic refinement, e.g., to refine prismatic elements within boundary layers preferentially along a single axis.

We rely on the following properties to compute the distribution of elements and trees of a forest:

1. Each process maintains a consecutive range of local trees. Its first and last local tree may be shared with other processes. The range may also be empty for a process, in which case its first local tree is the first local tree of the next non-empty process; in this case, the last local tree id is `first_local_tree_id-1`, as it has no valid first or last local tree. A process stores the shape of its local trees' root elements.
2. We maintain a global replicated array  $\mathfrak{R}[0, P]$  that contains the cumulative number of trees before any process  $p \in [0, P)$ , thus  $\mathfrak{R}_0 = 0$ ,  $\mathfrak{R}_P = K$ .
3. In order not to count any tree twice in  $\mathfrak{R}$ , we define one responsible process  $p_k$  for each tree  $k \in [0, K-1]$ . It is the lowest-id process that shares tree  $k$ . Empty processes can never be responsible for any tree (a difference to [\[7\]](#)).

**5.1. Forest partitioning with multiple shapes.** The construction of a new forest takes a coarse mesh and an initial uniform refinement level  $\ell$  as parameters. The goal of this algorithm is to build an equally partitioned forest of elements of level  $\ell$  exclusively. On input, the coarse mesh may be distributed in an arbitrary way. Since every process only creates elements of the forest in its local trees, we conclude that the input coarse mesh is in general not partitioned to allow for a fair distribution of elements. Thus, the first part of the forest construction is to compute the boundaries of each process, which are then used to fill the forest with its leaf elements.

For each shape of root elements, we can compute the number of elements in the associated tree on level  $\ell$  in  $O(1)$ , i.e., constant runtime. This number, however, might vary for each tree. Therefore, we let each process responsible for one or more trees

compute the number of elements  $N(\ell)$  each tree will hold at level  $\ell$  and store it for later reference. This local number of elements is communicated to all processes via an `MPI_Scan`, from which each process derives a local copy of the non-descending array  $\mathfrak{C}[0, P]$ ; for each process  $p$ , it holds the current element offset, i.e., the global index of the first element within the trees process  $p$  is responsible for. By construction, its final entry is the total number of elements:  $\mathfrak{C}_0 = 0$ ,  $\mathfrak{C}_P = N$ .

After repartitioning, the  $N$  elements shall be equally distributed among all  $P$  processes. In the resulting partitioning, we can determine the element range of process  $p$  by the familiar formula

$$(5.2) \quad O_p = \left\lfloor \frac{pN}{P} \right\rfloor, \quad N_p = O_{p+1} - O_p,$$

where  $O_0, \dots, O_P$  are the ideal element offsets and the value of  $N_p$  differs by at most one among all processes. The other way around, the element with global index  $E$  will belong to the process

$$(5.3) \quad p(E) = P - 1 - \left\lfloor \frac{P(N - 1 - E)}{N} \right\rfloor.$$

To achieve an equal distribution, the current tree- and element boundaries have to be shifted. To perform this shift, we determine the range of processes each process needs to send information about its trees to. Based on  $\mathfrak{C}$  we can compute the global indices  $T$  of the first elements of each tree of process  $p$  locally. We use (5.3) to compute the processes  $0 \leq q_0 \leq q_1 < P$  which need the boundary information of  $n_0 = T[0]$  and  $n_1 = T[K_p]$ , where  $K_p$  is the number of trees on process  $p$ . We use a binary search to find the processes  $q_0$  and  $q_1$ . The processes in the range  $[q_0, q_1]$  need information from process  $p$  about its boundaries. Each of them will thus receive at least one message from process  $p$ .

The overall algorithm takes the following steps:

1. Compute the process-local number of elements.
2. Use a prefix reduction to produce an offset array  $\mathfrak{C}$ .
3. Produce an array  $T$ , where entry  $T_i$  is the global index of the first element of local tree  $i$ .
4. For each local tree  $i$ , compute the smallest process number requiring information about its elements (via a binary search in  $T$ ).
5. Each process computes the up to two processes it retrieves information from.
6. Send tree- and element boundaries to each process for which we have information.

The details of the algorithm are presented in Algorithm 5.1. The performance of the algorithm, among others, is discussed in Section 6 and Section 7.

**6. Element performance.** In this set of tests we compare the performance of our pyramid implementation with the existing implementations of space-filling curves for standard elements in three dimensions.

To ensure a fair comparison between the different types of elements, we make sure that the number of elements created is roughly the same. For all types we create a uniform mesh consisting of several trees. It is then refined once and partitioned, before a ghost layer is created. The following setups are used for the tests:

- For pyramids we refine all elements of type 0, 2, 4, and 6. The initial mesh has eight trees and we start with a uniform mesh on level 7, 8, 9, or 10.

**Algorithm: uniform\_bounds**

**Data:** The calling process  $p$  computes the boundary information of a uniform partition based on the tree and elements it owns and sends the information to processes that need the information. It also receives this information.

```

index = global_index(first_tree(p))    ▷ Global index of the first element of proc  $p$ 
 $\mathcal{C}[p] = \text{index}$                       ▷ Array of offsets, use MPI_Scan
for  $i = 0, \dots, K_p$  do
  |  $T[i] = \text{first\_element}(\text{tree}(i))$     ▷ Array of global ids of first tree elements
end
 $q_0 = \text{proc\_to\_send}(T[0])$            ▷ Use (5.3), the first process to send to
 $q_1 = \text{proc\_to\_send}(T[K_p])$          ▷ Use (5.3), the last process to send to
 $\text{proc\_to\_tree} = \text{bsearch}(T, q_0, q_1)$  ▷ At  $q$ , the index of its 1st tree in  $T$ 
for  $q = q_0, \dots, q_1$  do
  | Note: Compute the first tree  $FT$  and last tree  $LT$  to send to  $q$ 
  |  $FE_q, LE_q$ , to be filled.           ▷ First and last element of  $q$ , use (5.2)
  | if  $is\_empty(q)$  then
  | |  $FT_q = FT_{\text{next-non-empty-proc}}$     ▷  $FT_q$  will be sent to  $q$ 
  | end
  |  $\text{first\_tree} = \text{proc\_to\_tree}[q]$      ▷ Possible first tree of  $q$ 
  |  $FE = T[\text{first\_tree}]$                ▷ Possible first element of  $q$ 
  | if  $FE \geq T[K_p]$  then
  | | skip to the next process           ▷ Proc  $p$  has no information for  $q$ 
  | else
  | | Note: Check if the calling process can send the lower or upper bound to  $q$ 
  | | if  $FE > FE_q$  then
  | | | continue                         ▷ The lower-bound info is on another proc
  | | else
  | | |  $FT_q = \text{shift}(\text{first\_tree})$      ▷ Shift by -1 if  $FE$  is on shared tree
  | | |  $FE_q = O_q - T[FT_q]$            ▷ Tree-local id of the first element of  $q$ 
  | | end
  | | if  $T(N) < LE_q$  then
  | | | continue                         ▷ The upper bound info is on another proc
  | | else
  | | |  $LT_q = \text{proc\_to\_tree}[q+1] - 1$  ▷ Set the last tree of  $q$ 
  | | |  $LE_q = O_{q+1} - T[LT_q] - 1$    ▷ Tree-local id of the last element of  $q$ 
  | | end
  | end
  | Send  $FT_q$  and  $LT_q$  to  $q$            ▷ Non-blocking send
end
 $q_{\text{recv\_first}}, q_{\text{recv\_last}} = \text{binary\_search}(\mathcal{C})$  ▷ Search procs that send to calling proc
 $\text{recv}(q_{\text{recv\_first}}, q_{\text{recv\_last}})$     ▷ Receive boundary information
Algorithm 5.1: Compute uniform bounds for an initial forest partition.

```

- For all other element types we refine every second element. The initial mesh has two trees and the uniform mesh has level 8, 9, 10, or 11.

We run three tests, each doubling the number of processes. That way, we can compare weak and strong scaling for each type of element. The results of this test series are summarized and visualized in Figures 6.1, 6.2, and 6.3. For the smallest examples we create  $143 \times 10^6$  (pyramids) or  $150 \times 10^6$  (other) elements in total, resulting in at least  $2 \times 10^6$  elements per process. The largest benchmark creates  $75 \times 10^9$  or  $77 \times 10^9$  elements, respectively.

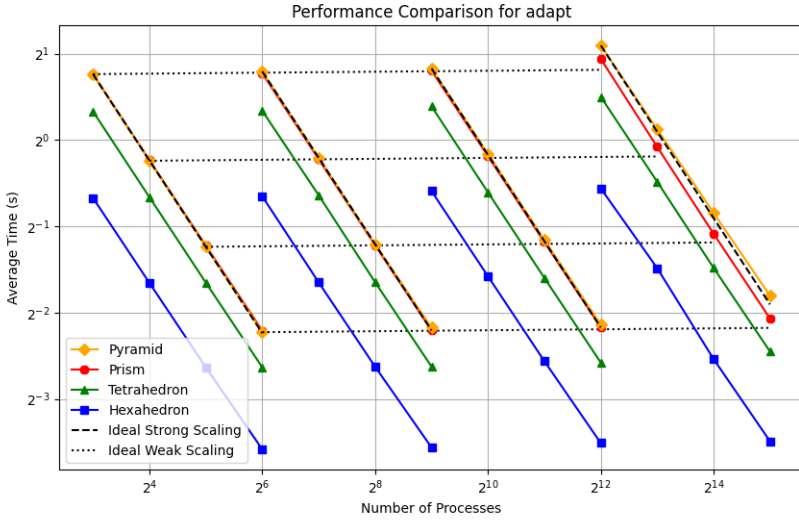


Fig. 6.1: The runtimes of the `Adapt` algorithm executed for four different problem sizes. We demonstrate near ideal strong and weak scaling for all types of elements.

All experiments have been executed on CARA, a high-performance cluster run by the German Aerospace Center (DLR). It has 2168 nodes with two AMD EPYC 7601 (32 cores, 2.2 GHz) each. Each node has access to 128 GB DDR4 (2666 MHz) RAM. An Infiniband HDR network connects the nodes [12].

For all core algorithms of `t8code` we observe a similar scaling behavior between pyramids and the other element shapes. Especially for the `Partition` and the `Adapt` algorithms we observe nearly ideal strong and weak scaling.

For the `New` algorithm the strong scaling is nearly ideal too; however, we observe a small jump in the runtime for the two largest configurations for the pyramidal algorithms. We suspect to have reached a near worst-case scenario for the boundaries in the pyramidal case. It results in a more costly communication pattern, increasing the runtime.

In general, the algorithms for pyramids are a bit more costly, which is caused by the increased complexity of the calculations at the element level. However, for forest-level algorithms that do not prompt weighty per-element computation, the runtime is similar to other non-hexahedral elements. Hexahedra run the fastest, because the element-level algorithms do not have to consider different element types or type-dependent branching. In fact, the hexahedral element routines are the only code linked in from `p4est`, wrapped in `t8code`'s virtual function interface, but we would expect a native `t8code` implementation to be of similar speed. All in all, we preserve the near ideal scaling behavior of `t8code` for all types of elements, including the pyramids introduced in this work.

The runtime analysis of the `Ghost` algorithm [21] is complex: The determination of ghost elements involves a depth-first search, leading to an added logarithmic factor in terms of the elements per process. On the other hand, the size of the ghost layer itself, which represents a surface area, grows with an exponent of  $2/3$  compared to the element count of a process. As the focus of this work is not the `Ghost` algorithm, we

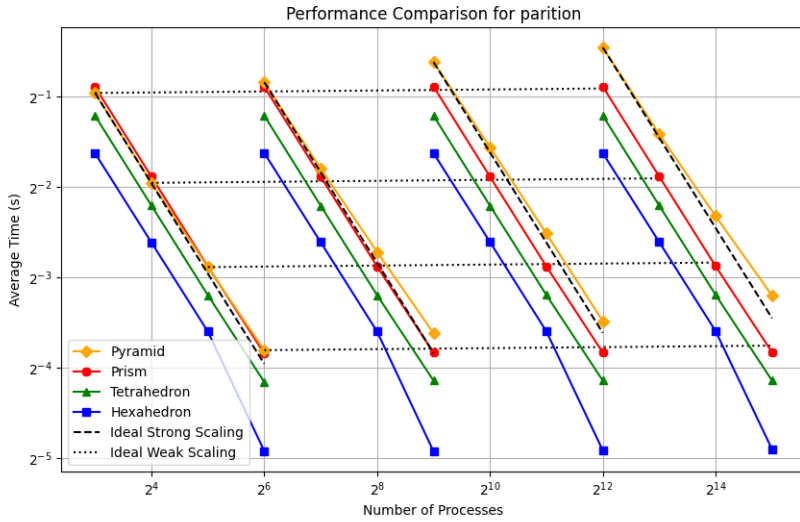


Fig. 6.2: An evaluation of strong and weak scaling of the Partition algorithm of  $\tau 8$ code for various element shapes. The configuration is noted below in Figure 6.3.

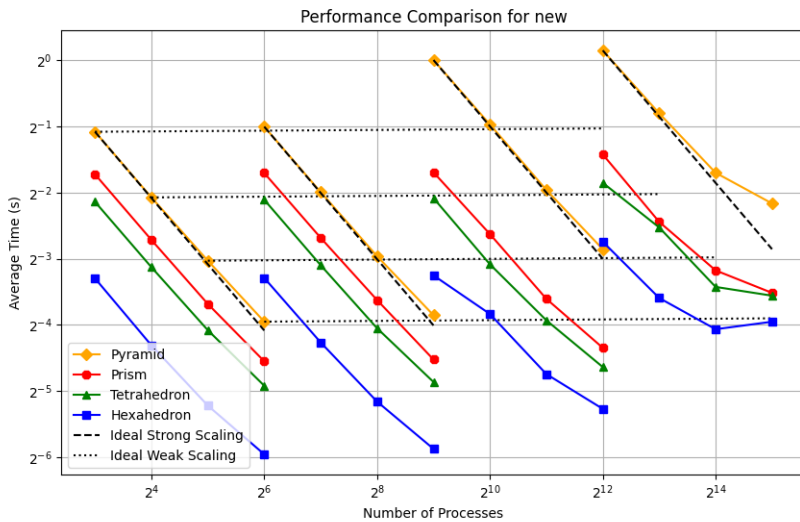


Fig. 6.3: A performance evaluation of the New algorithm of  $\tau 8$ code (Algorithm 5.1). We create a forest with a small number of trees and prescribe a uniform refinement of at least level 7. For each level we double the number of processes. After doubling the number of processes three times we increase the level of the uniform forest once. The ideal scaling for pyramids is not constant, because the number of pyramids in a mesh increases by a factor of greater than 8 on average when uniformly refining.

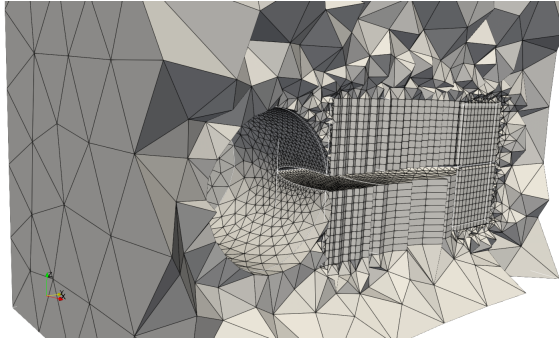


Fig. 7.1: The mesh used for the benchmarks in Section 7. It is a toy example of an airplane geometry with a single wing. The mesh consists of 69,431 tetrahedra, 3,800 hexahedra, 29,520 prisms and 3,120 pyramids. The mesh can be found in [33]. The elements near the “foil” are extruded prisms, the far field consist of tetrahedra. At the boundary, hexahedra and pyramids occur, resulting in a suitable hybrid CFD mesh.

Processes	$2^{14}$	$2^{15}$	$2^{16}$	$2^{17}$
Total runtime / s	250.262	126.602	69.943	49.942
Adapt runtime / s	224.099	111.728	57.835	36.083
Adapt / Total	89.54%	88.65%	83.81%	72.27%

Table 7.1: The total runtime of the hybrid mesh example. Between 72% and 90% of this runtime is spent in `Adapt`. The runtime of the algorithm depends on the cost of the adaptation criterion. In comparison to the criterion used in Section 6, this geometric criterion to refine in the vicinity of a moving virtual wall is more costly.

omit a detailed runtime discussion. Nonetheless, we present the runtime at a glance in [SM2.1](#) and [SM2.2](#), demonstrating that the inclusion of pyramidal elements performs comparably to existing elements and does not introduce additional computational overhead within an application.

**7. Hybrid mesh example.** In this section, we use a hybrid mesh to demonstrate the performance and scalability of Algorithm 5.1, the `New` algorithm introduced in Section 5.1. The coarse mesh is depicted in Figure 7.1; it consists of around 100,000 trees, containing all 3D element shapes supported by `t8code`. Initially, the mesh is refined five times. During adaptation, all elements inside a virtual skewed wall are refined twice. After partitioning and the computation of the ghost layer, the wall is moved and we adaptively refine again. In total, the wall is moved five times and we construct a refined mesh consisting of up to  $40 \times 10^9$  elements.

The test has been performed on CARO [13], a high performance cluster run by the German Aerospace Center. It is the sister system of CARA, which was in downtime and therefore not available for this test. CARO consists of 1,276 nodes with two AMD EPYC 7702 (64 cores, 2.0 GHz) each. Each node we used has access to 256 GB DDR4 (3200 MHz) RAM. The nodes are connected via an Infiniband HDR network.

Table 7.1 illustrates the results of the experiments: The total runtime of each test is shown for up to 131,072 processes. Most of the time is used to evaluate the adaptation criterion, which is an expensive one in this case. Each element has to test

whether it is inside the wall, or not.

The runtime of the other core algorithms of `t8code` are negligible in comparison, because they do not perform any geometry evaluation. Here it suffices to gather information about the elements in the reference space.

For the first three runs, each process contains more than a million elements, and a near ideal strong scaling can be observed. For the last run ( $2^{17}$  processes), the scaling is slightly less than ideal, since the number of elements drops down to roughly 300,000 elements per process and the communication overhead becomes noticeable.

**8. Conclusion.** In this work, we have successfully introduced and formalized a novel space-filling curve for pyramidal elements. We demonstrated, through a rigorous reference implementation, how to integrate pyramids into tree-based, hybrid adaptive mesh-refinement software. This advancement is significant because it enables pyramids to function effectively as a bridge element within scalable tree-based hybrid meshes, significantly increasing the geometric flexibility and robustness of meshes used for complex simulations. Furthermore, we introduce a new algorithm to compute uniform bounds for the initial partitioning of a hybrid mesh.

We executed extensive tests to demonstrate the scalability and efficiency of our design. The core algorithms of `t8code` maintain the same favorable performance characteristics for pyramid elements as they do for the existing hexahedral, tetrahedral, and prismatic elements. We further demonstrate this capability through the parallel efficiency of `t8code` on a large-scale hybrid mesh (over 100,000 trees), utilizing up to 131,072 processes. In summary, this work establishes an efficient and scalable foundation for hybrid adaptive mesh refinement (AMR).

In future works, we plan to simplify the existing Morton-type SFC implementations across all standard element shapes, through a unified theory that can potentially yield further performance improvements. Second, we intend to integrate this hybrid tree-based AMR infrastructure into common numerical solver libraries to provide a tangible improvement with respect to indexing, data locality, and parallel efficiency.

**Acknowledgements.** We acknowledge funding by the DFG under grant no. 467255783 (“Hybride AMR-Simulationen”). We acknowledge travel funds by the Hausdorff Center for Mathematics (HCM) at the University of Bonn. The HCM is funded by the German Research Foundation (DFG) under Germany’s excellence initiative EXC 59 – 241002279 (“Mathematics: Foundations, Models, Applications”).

We chose equal-weighted scientific color maps [14], and employed Gemini Thinking 3 Pro to polish the general style of the paper.

## REFERENCES

- [1] M. F. W. BANGERTH, *Algorithms for parallel generic hp-adaptive finite element software*, ACM Transactions on Mathematical Software, 47 (2023), pp. 1–26, <https://doi.org/10.1145/3603372>.
- [2] W. BANGERTH, C. BURSTEDDE, T. HEISTER, AND M. KRONBICHLER, *Algorithms and data structures for massively parallel generic adaptive finite element codes*, ACM Transactions on Mathematical Software, 38 (2011), pp. 1–28, <https://doi.org/10.1145/2049673.2049678>.
- [3] W. BANGERTH, R. HARTMANN, AND G. KANSCHAT, *deal.II – a general-purpose object-oriented finite element library*, ACM Transactions on Mathematical Software, 33 (2007), pp. 24–50, <https://doi.org/10.1145/1268776.1268779>.
- [4] J. BEY, *Der BPX-Vorkonditionierer in drei Dimensionen: Gitterverfeinerung, Parallelisierung und Simulation*, 1992. Preprint.
- [5] E. BOMAN, U. CATALYUREK, C. CHEVALIER, AND K. DEVINE, *The Zoltan and Isorropia parallel toolkits for combinatorial scientific computing: Partitioning, ordering and coloring*,

- Scientific Programming, 20 (2012), pp. 129–150, <https://doi.org/10.1155/2012/713587>.
- [6] C. BURSTEDDE, **p4est**: *Parallel AMR on forests of octrees*, 2010. <https://www.p4est.org/> (last accessed June 18th, 2025).
- [7] C. BURSTEDDE, *Parallel tree algorithms for AMR and non-standard data access*, ACM Transactions on Mathematical Software, 46 (2020), pp. 1–31, <https://doi.org/10.1145/3401990>.
- [8] C. BURSTEDDE AND J. HOLKE, *A tetrahedral space-filling curve for nonconforming adaptive meshes*, SIAM Journal on Scientific Computing, 38 (2016), pp. C471–C503, <https://doi.org/10.1137/15M1040049>.
- [9] C. BURSTEDDE AND J. HOLKE, *Coarse mesh partitioning for tree-based AMR*, SIAM Journal on Scientific Computing, 39 (2017), pp. C364–C392, <https://doi.org/10.1137/16M1103518>.
- [10] C. BURSTEDDE, M. KIRILIN, AND R. KLÖFKORN, *A new DUNE grid for scalable dynamic adaptivity based on the p4est software library*, 2025, <https://arxiv.org/abs/2507.11386>.
- [11] C. BURSTEDDE, L. C. WILCOX, AND O. GHATTAS, **p4est**: *Scalable algorithms for parallel adaptive mesh refinement on forests of octrees*, SIAM Journal on Scientific Computing, 33 (2011), pp. 1103–1133, <https://doi.org/10.1137/100791634>.
- [12] *High-performance computer cara*. <https://www.dlr.de/de/forschung-und-transfer/forschungsinfrastruktur/grossforschungsanlagen/hpc-cluster/cara>.
- [13] *High-performance computer caro*. <https://www.dlr.de/de/forschung-und-transfer/forschungsinfrastruktur/grossforschungsanlagen/hpc-cluster/caro>.
- [14] F. CRAMERI, *Scientific colour maps*, 2023, <https://doi.org/10.5281/zenodo.8409685>.
- [15] D. DAVYDOV, T. GERASIMOV, J.-P. PELTERET, AND P. STEINMANN, *Convergence study of the h-adaptive pum and the hp-adaptive fem applied to eigenvalue problems in quantum mechanics*, Advanced Modeling and Simulation in Engineering Sciences, 7 (2017), <https://doi.org/10.1186/s40323-017-0093-0>.
- [16] B. E. FELDMAN, J. F. O'BRIEN, AND B. M. KLINGNER, *Animating gases with hybrid meshes*, ACM Trans. Graph., 24 (2005), p. 904–909, <https://doi.org/10.1145/1073204.1073281>.
- [17] M. GRIEBEL AND G. W. ZUMBUSCH, *Parallel multigrid in an adaptive PDE solver based on hashing and space-filling curves*, Parallel Computing, 25 (1999), pp. 827–843, [https://doi.org/10.1016/S0167-8191\(99\)00020-4](https://doi.org/10.1016/S0167-8191(99)00020-4).
- [18] D. HILBERT, *Über die stetige Abbildung einer Linie auf ein Flächenstück*, Mathematische Annalen, 38 (1891), pp. 459–460, [https://doi.org/10.1007/978-3-662-38452-7\\_1](https://doi.org/10.1007/978-3-662-38452-7_1).
- [19] J. HOLKE, *Scalable algorithms for parallel tree-based adaptive mesh refinement with general element types*, PhD thesis, Rheinische Friedrich-Wilhelms-Universität Bonn, 2018, <http://d-nb.info/1173789790/34>. <https://bonndoc.ulb.uni-bonn.de/xmlui/handle/20.500.11811/7661>.
- [20] J. HOLKE, C. BURSTEDDE, D. KNAPP, L. DREYER, S. ELSWEIJER, V. UENLUE, J. MARKERT, I. LILIKAKIS, AND N. BOEING, **t8code**: *Parallel AMR on hybrid non-conforming meshes*, 2015, <https://doi.org/10.5281/zenodo.7034838>. <http://github.com/DLR-AMR/t8code>, last accessed January 20th, 2023, 10.5281/zenodo.7034838.
- [21] J. HOLKE, D. KNAPP, AND C. BURSTEDDE, *An optimized, parallel computation of the ghost layer for adaptive hybrid forest meshes*, 2019, <https://arxiv.org/abs/1910.10641>.
- [22] T. ISAAC AND M. G. KNEPLEY, *Support for non-conformal meshes in PETSc's DMPlex interface*, 2015, <https://arxiv.org/abs/1508.02470>.
- [23] Y. ITO AND K. NAKAHASHI, *Improvements in the reliability and quality of unstructured hybrid mesh generation*, International Journal for Numerical Methods in Fluids, 45 (2004), pp. 79–108, <https://doi.org/10.1002/fld.669>.
- [24] Y. ITO, A. M. SHIH, B. K. SONI, AND K. NAKAHASHI, *An approach to generate high quality unstructured hybrid meshes*, 44th AIAA Aerospace Sciences Meeting and Exhibit, (2006), <https://doi.org/10.2514/6.2006-530>.
- [25] Y. KALLINDERIS AND C. KAVOUKLIS, *A dynamic adaptation scheme for general 3-d hybrid meshes*, Computer Methods in Applied Mechanics and Engineering, 194 (2005), pp. 5019–5050, <https://doi.org/10.1016/j.cma.2004.11.023>. Unstructured Mesh Generation.
- [26] G. KARYPIS AND V. KUMAR, **METIS** – *Unstructured Graph Partitioning and Sparse Matrix Ordering System, Version 2.0*, 1995.
- [27] G. KARYPIS, K. SCHLOEGEL, AND V. KUMAR, **Parmetis**: *Parallel graph partitioning and sparse matrix ordering library*, 01 1997.
- [28] N. KASMAI, D. THOMPSON, E. LUKE, M. JANKUN-KELLY, AND R. MACHIRAJU, *Feature-based adaptive mesh refinement for wingtip vortices*, International Journal for Numerical Methods in Fluids, 66 (2011), pp. 1274–1294, <https://doi.org/doi.org/10.1002/fld.2312>.
- [29] A. KHAWAJA, T. MINYARD, AND Y. KALLINDERIS, *Adaptive hybrid grid methods*, Computer Methods in Applied Mechanics and Engineering, 189 (2000), pp. 1231–1245, [https://doi.org/10.1016/S0045-7825\(99\)00375-8](https://doi.org/10.1016/S0045-7825(99)00375-8). Adaptive Methods for Compressible CFD.

- [30] A. C. KIRBY, M. J. BRAZELL, Z. YANG, R. ROY, B. R. AHRABI, M. K. STOELLINGER, J. SITARAMAN, AND D. J. MAVRIPLIS, *Wind farm simulations using an overset hp-adaptive approach with blade-resolved turbine models*, The International Journal of High Performance Computing Applications, 33 (2019), pp. 897–923, <https://doi.org/10.1177/1094342019832960>.
- [31] D. KNAPP, *Adaptive Verfeinerung von Prismen*, Bachelor's thesis, Rheinische Friedrich-Wilhelms-Universität Bonn, 2017.
- [32] D. KNAPP, *A space-filling curve for pyramidal adaptive mesh refinement*, Master's thesis, Rheinische Friedrich-Wilhelms-Universität Bonn, 2020.
- [33] D. KNAPP, J. HOLKE, J. FUSSBROICH, S. ELSWEIJER, AND O. ALBERS, *t8data*, 2025. <https://github.com/DLR-AMR/t8data>.
- [34] H. L. LEBESGUE, *Leçons sur l'intégration et la recherche des fonctions primitives*, Gauthier-Villars, 1904.
- [35] MESSAGE PASSING INTERFACE FORUM, *MPI: A message-passing interface standard, version 3.1*, 2015, <http://www.mpi-forum.org/docs/mpi-3.1/mpi31-report.pdf>.
- [36] G. M. MORTON, *A computer oriented geodetic data base; and a new technique in file sequencing*, tech. report, IBM Ltd., 1966.
- [37] G. PEANO, *Sur une courbe, qui remplit toute une aire plane*, Math. Ann., 36 (1890), pp. 157–160, <https://doi.org/10.1137/100799071>.
- [38] F. PELLEGRINI, *Scotch and PT-Scotch Graph Partitioning Software: An Overview*, in Combinatorial Scientific Computing, O. S. Uwe Naumann, ed., Chapman and Hall/CRC, 2012, pp. 373–406, <https://doi.org/10.1201/b11644-15>, <https://inria.hal.science/hal-00770422>.
- [39] H. RANOCHA, M. SCHLOTTKE-LAKEMPER, A. R. WINTERS, E. FAULHABER, J. CHAN, AND G. GASSNER, *Adaptive numerical simulations with Trixi.jl: A case study of Julia for scientific computing*, Proceedings of the JuliaCon Conferences, 1 (2022), p. 77, <https://doi.org/10.21105/jcon.00077>.
- [40] H. SAMET, *Foundations of multidimensional and metric data structures*, Elsevier/Morgan Kaufmann, 2006, [https://booksite.elsevier.com/samplechapters/9780123694461/Sample\\_Chapters/01~Frontmatter.pdf](https://booksite.elsevier.com/samplechapters/9780123694461/Sample_Chapters/01~Frontmatter.pdf).
- [41] W. SIERPIŃSKI, *Sur une nouvelle courbe continue qui remplit toute une aire plane*, Bulletin de l'Académie des Sciences de Cracovie, Séries A (1912), pp. 462–478, [https://doi.org/10.1007/978-3-7091-9537-6\\_6](https://doi.org/10.1007/978-3-7091-9537-6_6).
- [42] C. W. SMITH, M. RASQUIN, D. IBANEZ, K. E. JANSEN, AND M. S. SHEPHARD, *Improving unstructured mesh partitions for multiple criteria using mesh adjacencies*, SIAM Journal on Scientific Computing, 40 (2018), pp. C47–C75, <https://doi.org/10.1137/15M1027814>.
- [43] J. R. STEWART AND H. C. EDWARDS, *A framework approach for developing parallel adaptive multiphysics applications*, Finite Elements in Analysis and Design, 40 (2004), pp. 1599–1617, <https://doi.org/10.1016/j.finel.2003.10.006>.
- [44] H. SUNDAR, R. SAMPATH, AND G. BIROS, *Bottom-up construction and 2:1 balance refinement of linear octrees in parallel*, SIAM Journal on Scientific Computing, 30 (2008), pp. 2675–2708, <https://doi.org/10.1137/070681727>.
- [45] H. TROPF AND H. HERZOG, *Multidimensional range search in dynamically balanced trees*, Angewandte Informatik, 2 (1981), pp. 71–77.
- [46] T. TU, D. R. O'HALLARON, AND O. GHATTAS, *Scalable parallel octree meshing for terascale applications*, in SC '05: Proceedings of the International Conference for High Performance Computing, Networking, Storage, and Analysis, ACM/IEEE, 2005, pp. 4–4, <https://doi.org/10.1109/SC.2005.61>.
- [47] C. WALSHAW, M. CROSS, AND M. EVERETT, *Parallel dynamic graph partitioning for adaptive unstructured meshes*, Journal of Parallel and Distributed Computing, 47 (1997), pp. 102–108, <https://doi.org/10.1006/jpdc.1997.1407>.
- [48] M. WANG, Y. TANG, X. GUO, AND X. REN, *Performance analysis of the graph-partitioning algorithms used in openfoam*, in 2012 IEEE Fifth International Conference on Advanced Computational Intelligence (ICACI), 2012, pp. 99–104, <https://doi.org/10.1109/ICACI.2012.6463129>.
- [49] T. WEINZIERL AND M. MEHL, *Peano—a traversal and storage scheme for octree-like adaptive Cartesian multiscale grids*, SIAM Journal on Scientific Computing, 33 (2011), pp. 2732–2760, <https://doi.org/10.1137/100799071>.
- [50] M. ZHOU, O. SAHNI, K. D. DEVINE, M. S. SHEPHARD, AND K. E. JANSEN, *Controlling unstructured mesh partitions for massively parallel simulations*, SIAM Journal on Scientific Computing, 32 (2010), pp. 3201–3227, <https://doi.org/10.1137/090777323>.

## SUPPLEMENTARY MATERIALS: FORMULAS AND Ghost RUNTIME

DAVID KNAPP, JOHANNES HOLKE, THOMAS SPENKE, AND CARSTEN BURSTEDDE

**SM1. Uniform refinement of a root pyramid.** The formula for the number of descendants of a root pyramid at a given level  $\ell$  derives from the following recursion,

$$(SM1.1) \quad P(\ell + 1) = 4 \cdot 2^{3\ell} + 6P(\ell), \quad \text{where} \quad P(0) = 1.$$

If we expand it and simplify, we obtain the following result,

$$(SM1.2) \quad \begin{aligned} P(\ell) &= 4 \left( 6^0 2^{3(\ell-1)} + 6^1 2^{3(\ell-2)} + \dots + 6^{\ell-1} 2^0 \right) + 6^\ell \\ &= 4 \cdot 8^{\ell-1} \sum_{k=0}^{\ell-1} \left( \frac{3}{4} \right)^k + 6^\ell = 4 \cdot 8^{\ell-1} \frac{1 - (3/4)^\ell}{1 - 3/4} + 6^\ell \\ &= 2 \cdot 8^\ell - 6^\ell. \end{aligned}$$

It is easily verified using induction.

**SM2. Performance results of the Ghost algorithm.** We display strong scaling results for the ghost algorithm running our largest experiment in Table [SM2.1](#). Weak scaling results follow in Table [SM2.2](#).



Procs	elems / proc	avg. ghosts/proc	ghost time	runtime	
Pyramid				per elem	per ghost
4096	18.470e6	254K	2.477s	1.341e-7	9.751e-6
8192	9.235e6	169K	1.482s	1.604e-7	8.769e-6
16K	4.618e6	111K	1.029s	2.228e-7	9.270e-6
32K	2.309e6	75K	0.652s	2.707e-7	8.333e-6
Tetrahedron				per elem	per ghost
4096	18.874e6	274K	1.408s	7.490e-8	5.140e-6
8192	9.437e6	164K	0.723s	7.661e-8	4.441e-6
16K	4.719e6	104K	0.455s	9.516e-8	4.375e-6
32K	2.359e6	70K	0.347s	1.471e-7	4.957e-6
Hexahedron				per elem	per ghost
4096	18.874e6	230K	1.312s	6.951e-8	5.704e-6
8192	9.437e6	156K	0.865s	9.071e-8	5.487e-6
16K	4.719e6	99K	0.537s	1.138e-7	5.424e-6
32K	2.359e6	59K	0.320s	1.356e-7	5.423e-6
Prism				per elem	per ghost
4096	18.874e6	348K	2.517s	1.334e-7	7.232e-6
8192	9.437e6	194K	1.265s	1.340e-7	6.521e-6
16K	4.719e6	138K	0.843s	1.786e-7	6.109e-6
32K	2.359e6	90K	0.614s	2.602e-7	6.822e-6

TABLE SM2.1

*The strong scaling and parallel efficiency of the ghost algorithm for the largest configuration of the element benchmark.*



procs	$l$	elems/proc	avg. ghosts/proc	ghost time	runtime	
Pyramid					per elem	per ghost
64	7	2.246e6	50823	0.546s	2.431e-7	1.0743e-5
512	8	2.272e6	64757	0.609s	2.680e-7	9.404e-6
4096	9	2.292e6	72065	0.651s	2.840e-7	9.033e-6
32K	10	2.308e6	75245	0.652s	2.825e-7	8.665e-6
Tetrahedron					per elem	per ghost
64	8	2.359e6	55551	0.335s	1.420e-7	6.030e-6
512	9	2.359e6	64131	0.343s	1.454e-7	5.348e-6
4096	10	2.359e6	68431	0.346s	1.467e-7	5.056e-6
32K	11	2.359e6	70583	0.347s	1.491e-7	4.916e-6
Hexahedron					per elem	per ghost
64	8	2.359e6	46080	0.314s	1.331e-7	6.814e-6
512	9	2.359e6	53760	0.318s	1.348e-7	5.915e-6
4096	10	2.359e6	57600	0.318s	1.348e-7	5.521e-6
32K	11	2.359e6	59520	0.320s	1.357e-7	5.379e-6
Prism					per elem	per ghost
64	8	2.359e6	71640	0.609s	2.58e-6	7.971e-6
512	9	2.359e6	81876	0.611s	2.59e-6	7.463e-6
4096	10	2.359e6	86994	0.613s	2.60e-6	7.046e-6
32K	11	2.359e6	89553	0.614s	2.602e-6	6.856e-6

TABLE SM2.2

*The weak scaling and parallel efficiency of the ghost algorithm for the largest configuration of the element benchmark.*

